crystals

MDPI

Comparative Study on AC Susceptibility of YBa$_2$Cu$_3$O$_{7-\delta}$ Added with BaZrO$_3$ Nanoparticles Prepared via Solid-State and Co-Precipitation Method

Nurhidayah Mohd Hapipi [1], Jee Khan Lim [2], Soo Kien Chen [1,3,*], Oon Jew Lee [2], Abdul Halim Shaari [1], Mohd Mustafa Awang Kechik [1], Kean Pah Lim [1], Kar Ban Tan [4], Masato Murakami [5] and Muralidhar Miryala [5]

[1] Department of Physics, Faculty of Science, Universiti Putra Malaysia, 43400 UPM Serdang, Selangor, Malaysia; gs52310@student.upm.edu.my (N.M.H.); ahalim@upm.edu.my (A.H.S.); mmak@upm.edu.my (M.M.A.K.); limkp@upm.edu.my (K.P.L.)
[2] School of Fundamental Science, Universiti Malaysia Terengganu, 21030 Kuala Nerus, Terengganu, Malaysia; p3595@pps.umt.edu.my (J.K.L.); oonjew@umt.edu.my (O.J.L.)
[3] Institute of Advanced Technology, Universiti Putra Malaysia, 43400 UPM Serdang, Selangor, Malaysia
[4] Department of Chemistry, Faculty of Science, Universiti Putra Malaysia, 43400 UPM Serdang, Selangor, Malaysia; tankarban@upm.edu.my
[5] Shibaura Institute of Technology, 3 Chome-7-5 Toyosu, Koto, Tokyo 135-8548, Japan; masatomu@shibaura-it.ac.jp (M.M.); miryala1@shibaura-it.ac.jp (M.M.)
*   Correspondence: chensk@upm.edu.my

check for updates

Abstract: Polycrystalline samples of YBa$_2$Cu$_3$O$_{7-\delta}$ (Y-123) added with x mol% of BaZrO$_3$ (BZO) nanoparticles (x = 0.0, 2.0, 5.0, and 7.0) were synthesized using co-precipitation (COP) and solid-state (SS) method. X-ray diffraction (XRD) patterns showed the formation of Y-123 and Y-211 as the major and minor phases, respectively. The samples prepared using COP method showed higher weight percentage of Y-123 phase (≤98%) compared to the SS samples (≤93%). A peak corresponding to BZO was also found in the samples added with BZO nanoparticles. The increasing intensity of the BZO peak as the BZO amount increased showed the increasing amount of the unreacted nanoparticles in the samples. Refinement of unit cell lattice parameters indicated that all the samples have an orthorhombic crystal structure and there is no orthorhombic-tetragonal phase transformation. As observed using scanning electron microscopy (SEM), all the samples showed randomly distributed grains with irregular shape. The average grain size for the pure sample prepared using COP method is smaller (0.30 µm) compared with that of the pure SS sample (1.24 µm). Addition of 7.0 mol% BZO led to an increase of average grain size to 0.50 µm and 2.71 µm for the COP and SS samples, respectively, indicating grain growth. AC susceptibility (ACS) measurement showed a decrease in the onset critical temperature, $T_{\text{c-onset}}$ with BZO addition. Comparatively, $T_{\text{c-onset}}$ for the COP samples is higher than that of the SS samples. The value of Josephson's current, I_o increased up to 2.0 mol% BZO addition, above which the I_o decreased more drastically for the SS samples. The value of I_o is 53.95 µA and 32.08 µA for the 2.0 mol% BZO added SS and COP samples, respectively. The decrease of I_o is attributed to the distribution of BZO particles at the grain boundaries as also reflected in the drastic decrease of phase lock-in temperature, T_{cj}. As a result of smaller average grain size, the presence of more grain boundaries containing insulating BZO particles led to lower I_o in the COP samples.

Keywords: AC susceptibility; BaZrO$_3$; co-precipitation; solid-state; YBa$_2$Cu$_3$O$_{7-\delta}$

1. Introduction

Yttrium-barium-copper-oxide, YBCO is the first type-II high temperature superconductor (HTS) that has been discovered to be superconducting above the boiling point of liquid nitrogen. Among the family members of YBCO, 123 phase (Y-123) shows the highest onset of superconductivity at around 90 K. In order for Y-123 to be more feasible for a wide range of applications, numerous studies have been undertaken to improve its critical temperature, T_c and critical current density, J_c [1–3]. In this regard, addition of chemical dopants is one of the most straight forward strategies. It was shown that the addition of $BaZrO_3$ (BZO) nanoparticles into Y-123 improved J_c without affecting much the T_c value [4,5]. This is because BZO did not dope into the structure of Y-123. Instead, they either remained unreacted within the matrix or reacted with Y-123 to form nano-precipitates leading to enhanced flux pinning [6].

Intensive research on fabrication of BZO doped YBCO films was conducted in the past [7–11]. However, limited study of BZO doped YBCO bulks has been reported so far [5,12]. From the perspective of large scale applications, it is essential to investigate the effects of synthesis route and dopant additions on the superconducting properties of YBCO bulks. There are several methods used to synthesize the materials. For example, solid-state (SS) method [13,14] and wet method such as sol-gel [15], co-precipitation (COP) [16–18], and thermal treatment [19]. In particular, COP is a highly desirable chemical method used to prepare nanomaterials. The powders obtained by COP method show smaller grain size, higher purity, and better homogeneity compared to that obtained using SS method [20,21]. Moreover, multiple calcination and regrinding process is unnecessary to obtain a good superconducting phase for the COP method [17,22]. Previously, we successfully synthesized YBCO added with nano BZO using COP method [23]. Therefore, we are motivated to carry out a comparative study on structural and superconducting properties of BZO nanoparticles added Y-123 prepared via SS method and COP method. COP can be defined as the process of carrying down a precipitate of substances which are normally soluble under the suitable conditions [24] and the starting materials can be metal acetates or metal nitrates [14].

2. Materials and Methods

Samples with nominal composition of $YBa_2Cu_3O_{7-\delta}$ (Y-123) added with x mol% of $BaZrO_3$ (BZO) nanoparticles (x = 2.0, 5.0, and 7.0) were prepared using solid state (SS) method and co-precipitation (COP) method, respectively.

2.1. Solid-State (SS) Method

To start with, Y_2O_3 (99.9%, Alfa Aesar, Ward Hill, Massachusetts, USA), $BaCO_3$ (99.8%, Alfa Aesar, Ward Hill, Massachusetts, USA) and CuO (99.9%, Strem Chemical, Newburyport, Massachusetts, USA) with the stoichiometric ratio of Y:Ba:Cu (1:2:3) were mixed and hand-ground for 1 h using a mortar and pestle. Then, the grounded mixture was calcined in air at 940 °C for 12 h. After calcination, the powders were reground for 1 h before adding x mol% (x = 2.0, 5.0, and 7.0, respectively) of $BaZrO_3$ nanoparticles (BZO, >50 nm, 98.5%, Sigma-Aldrich). The mixed powders were reground again and then pressed into circular pellets (~13-mm diameter and 2-mm thickness) by using a hydraulic press with an applied pressure load of five tons. Finally, the pellets were sintered at 950 °C for 12 h and slowly cooled to 450 °C for 12 h at the rate of 1 °C/min under oxygen flow before further cooling to room temperature. Pure samples (x = 0.0) were also prepared according to the same procedure to serve as reference for the purpose of comparison.

2.2. Co-Precipitation (COP) Method

For COP method, appropriate amounts of $Y(CH_3COO)_3 \cdot 4H_2O$ (99.9% Alfa Aesar), $Ba(CH_3COO)_2$ (≥99% Alfa Aesar), and $Cu(CH_3COO)_2 . H_2O$ (≥99% Sigma Aldrich) according to the stoichiometric ratio of Y:Ba:Cu (1:2:3) were dissolved in acetic acid to form solution A. To prepare solution B, oxalic acid

was dissolved in a mixture of distilled water: 2-propanol (1:1.5). Both solutions A and B were stirred at 300 rpm for 2 h before being cooled in an ice bath. The mixed solution A and B was filtered and dried at 100 °C for 12 h. The obtained dried powders were ground and calcined in air at 900 °C for 24 h. After that, appropriate amount of *x* mol% (*x* = 2.0, 5.0, and 7.0, respectively) $BaZrO_3$ nanoparticles (BZO, >50 nm, 98.5%, Sigma-Aldrich) was added to the calcined powders for mixing and grinding. Then, the mixture was pressed into circular pellets (~13-mm diameter and 2-mm thickness) by using a hydraulic press with an applied pressure load of 5 tons. Lastly, the pellets were sintered at 920 °C for 15 h and slowly cooled to 650 °C for 8 h (annealing process) before further cooling to room temperature. The sintering and annealing were done under a constant oxygen flow. Pure samples (*x* = 0.0) were also prepared according to the same procedure to serve as reference for the purpose of comparison.

2.3. Sample Characterization

Phase formation and crystal structure of the samples were examined by X-ray diffraction (XRD) method using the PW 3040/60 MPD X'Pert Pro Panalytical Philips DY 1861 X-ray diffractometer with Cu-K$_\alpha$ radiation source. Scanning was carried out in 2θ mode over the range of 20°–80° with the increment step size of 0.03°. The XRD data was analyzed using the X'pert HighScore Plus software. Surface morphology of the pellets was observed using a scanning electron microscope (SEM-LEO 1455 VPSEM). Superconducting properties of the samples were measured using the commercial AC Susceptometer of CryoBIND (cryogenic balanced inductive detector) SR830 at the frequency of 219 Hz and applied field of 0.5 Oe. Uncertainty of the AC Susceptometer is ±0.1 K.

3. Discussion

3.1. X-ray Diffraction (XRD) Analysis

Figure 1 shows the XRD patterns of the samples prepared via SS method and COP method, respectively. The XRD patterns were indexed to Y-123 phase with orthorhombic crystal structure and space group *Pmmm* (ICSD: 01-078-2143). Peaks with the highest intensity for both the SS and COP samples were indexed with the Miller indices of (0 1 3) and (1 0 3). Rietveld refinement was undertaken on the XRD data using the X'pert HighScore Plus software. Accordingly, the refined unit cell lattice parameters indicated that all the samples have an orthorhombic crystal structure. Hence, no structural transformation from orthorhombic to tetragonal phase was occurred as a result of BZO addition. By using the similar refinement method, fraction of different phases (in weight percentage) in the samples was obtained. Compared to SS method, the samples prepared using COP method have higher weight percentage of Y-123 phase in agreement with previous findings [20,21]. Table 1 indicates the weight percentage of Y-123 phase for the pure SS and COP samples is 93.2% and 97.5%, respectively. However, the weight percentage of Y-123 phase for the SS samples and COP samples started to decrease with the increasing of BZO additions. Some minor peaks of Y_2BaCuO_5 (Y-211) (ICSD: 01-079-0697) were also observed in the XRD patterns of all the samples. The presence of Y-211 phase may due to the synthesis condition such as the heat treatment process and the preparation of the material itself [25]. A peak corresponding to $BaZrO_3$ (BZO) (ICSD: 01-074-1299) started to appear at 2.0 mol% BZO addition and became more intense with increasing of BZO addition. This observation confirmed the distribution of BZO in the samples [26]. The increased intensity of the peak with increasing BZO addition suggests the saturation of solid solubility of BZO in Y-123 [27].
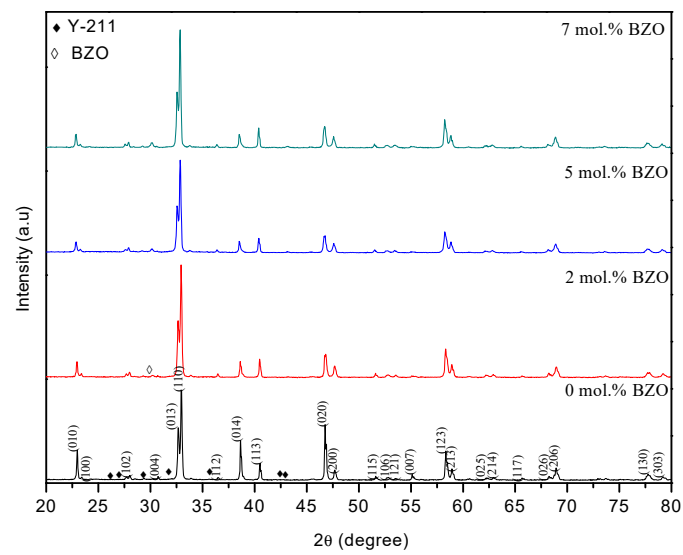
(**a**)
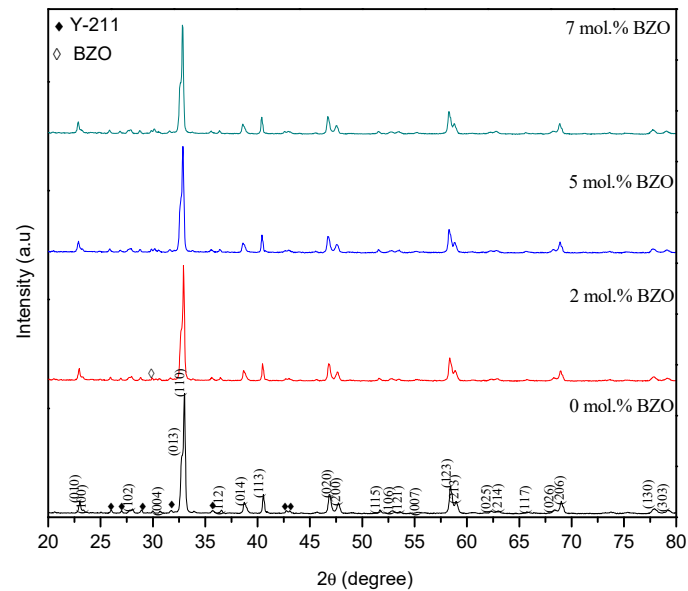
(**b**)

Figure 1. X-ray diffraction patterns of Y-123 + *x* mol% of BZO samples prepared via (**a**) SS method and (**b**) COP method. The Y-211 and BZO are marked with (♦) and (◊), respectively.

Table 1. Percentages of Y-123, Y-211, and BZO phases for Y-123 + *x* mol% of BZO samples prepared via SS method and COP method.

| BZO *x* (mol%) | Weight Percentage of Phases (%) | | | | | |
| | SS Method | | | COP Method | | |
	Y-123	Y-211	BZO	Y-123	Y-211	BZO
0.0	93.2	6.8	0.0	97.5	2.5	0.0
2.0	92.9	6.6	0.5	96.6	3.1	0.3
5.0	92.8	5.7	1.5	94.8	4.1	2.7
7.0	92.8	3.8	3.4	94.3	3.0	2.7

Table 2 summarizes crystallite size calculated based on the (103) peak of Y-123 using the Scherrer equation [28]:

$$L = \frac{K\lambda}{B_{size}COS\theta} \tag{1}$$

where L is the crystallite size, K is a dimensionless shape factor (0.9), B_{size} is line broadening at half of the maximum intensity (FWHM) in radian, λ is the X-ray wavelength for Cu-K$_\alpha$ radiation (1.5406 Å) and θ is Bragg angle in degree. Table 2 shows that the crystallite size of the SS samples is larger than that of the COP samples. Crystallite size of the pure SS and COP samples is 101.61 nm and 63.66 nm, respectively. Upon addition of BZO, the crystallite size increased for the COP samples. The larger crystallite size may be due to the bridging of fine particles that formed the continuous grain boundary networks [29]. Conversely, crystallite size became smaller for the SS samples with addition of BZO. Previously, the crystalline size of CaTiO$_3$ (CTO) was found to decrease possibly due to large difference in ionic radii between the dopant ion and host ion (Ti^{4+}) [30]. The nanocrystalline CTO was synthesized using soft chemical method followed by annealing. For our work, however, the same BZO nanoparticles were used for addition into the samples prepared by SS method and COP method. Judging from the data given in Table 2, the decrease in crystalline size for the BZO added SS samples is believed to be due to larger difference of the crystalline size between the BZO and Y-123 compared to that between the BZO and Y-123 prepared using COP method.

Table 2. FWHM of (103) peak, crystallite size and average grain size for Y-123 + *x* mol% of BZO samples calculated using Scherrer method. The average grain size of the samples was calculated from the randomly selected 100 grains of the SEM image.

BZO *x* (mol%)	FWHM of (103) Peak (°)	SS Method Crystallite Size (nm)	Average Grain Size, D (µm)	FWHM of (103) Peak (°)	COP Method Crystallite Size (nm)	Average Grain Size, D (µm)
0.0	0.1315	101.61	1.24 ± 0.14	0.1801	63.66	0.30 ± 0.01
2.0	0.1424	89.62	1.77 ± 0.06	0.1737	66.94	0.39 ± 0.02
5.0	0.1515	81.56	2.29 ± 0.01	0.1793	64.03	0.45 ± 0.02
7.0	0.1436	88.44	2.71 ± 0.11	0.1729	67.36	0.02

3.2. Microstructure Analysis

Figure 2 shows the SEM images of the SS and COP samples. All the samples have irregular shape and randomly distributed grains. The SEM images also show the increment in number of pores with BZO addition suggesting more porous structure for both SS and COP samples added with BZO. For calculation of average grain size, 100 grains were selected randomly from each SEM image and measured using the Image-J software. Figure 3 shows the distribution of grain size of the SS and COP samples. The average grain size is 1.24 µm and 0.30 µm, for the pure samples prepared via the SS method and COP method, respectively (Table 2). Addition of BZO into Y-123 sample increased the average grain size of the samples especially for the SS samples. The average grain size increased to 2.71 µm and 0.50 µm for the 7.0 mol% BZO added SS and COP samples, respectively. The increasing grain size is probably due to dispersion of BZO nanoparticles between the grains of Y-123 which promoted grain growth [5,31]. According to Table 2, the powders obtained by the COP method have smaller size and narrower size range (0.30–0.50 µm) in comparison with that obtained via the SS method (1.24–2.71 µm). This may be partly associated with the higher sintering temperature used in the SS method (950 °C, compared with 920 °C used for the COP method) leading to larger grain growth [21].
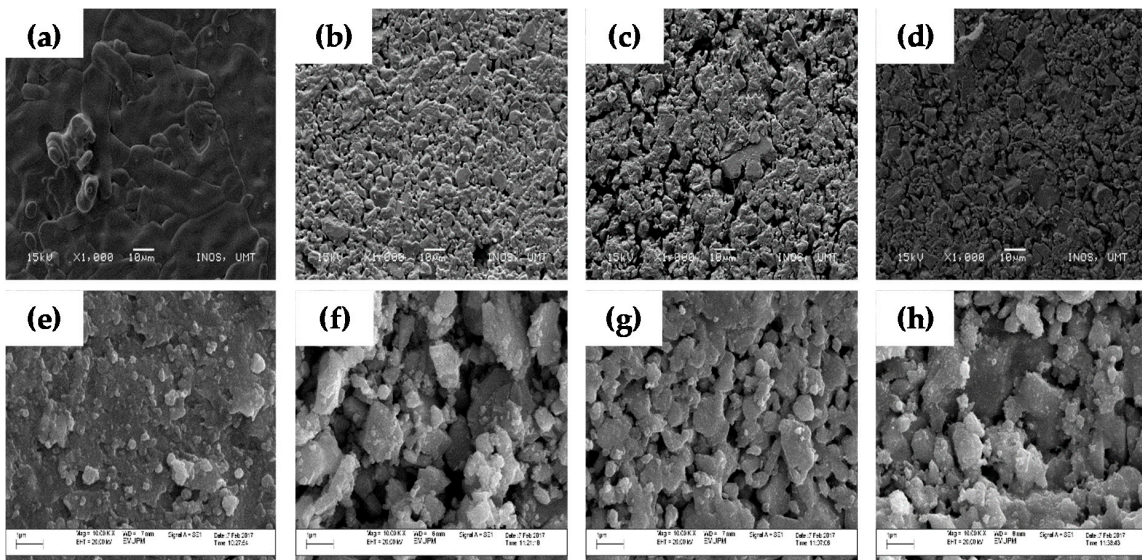
Figure 2. SEM images of Y-123 added with (**a**) 0.0 mol%, (**b**) 2.0 mol%, (**c**) 5.0 mol%, and (**d**) 7.0 mol% of BZO at 5000× magnification prepared via SS method. Bottom: SEM images of Y-123 added with (**e**) 0.0 mol%, (**f**) 2.0 mol%, (**g**) 5.0 mol%, and (**h**) 7.0 mol% of BZO at 5000× magnification prepared via COP method.
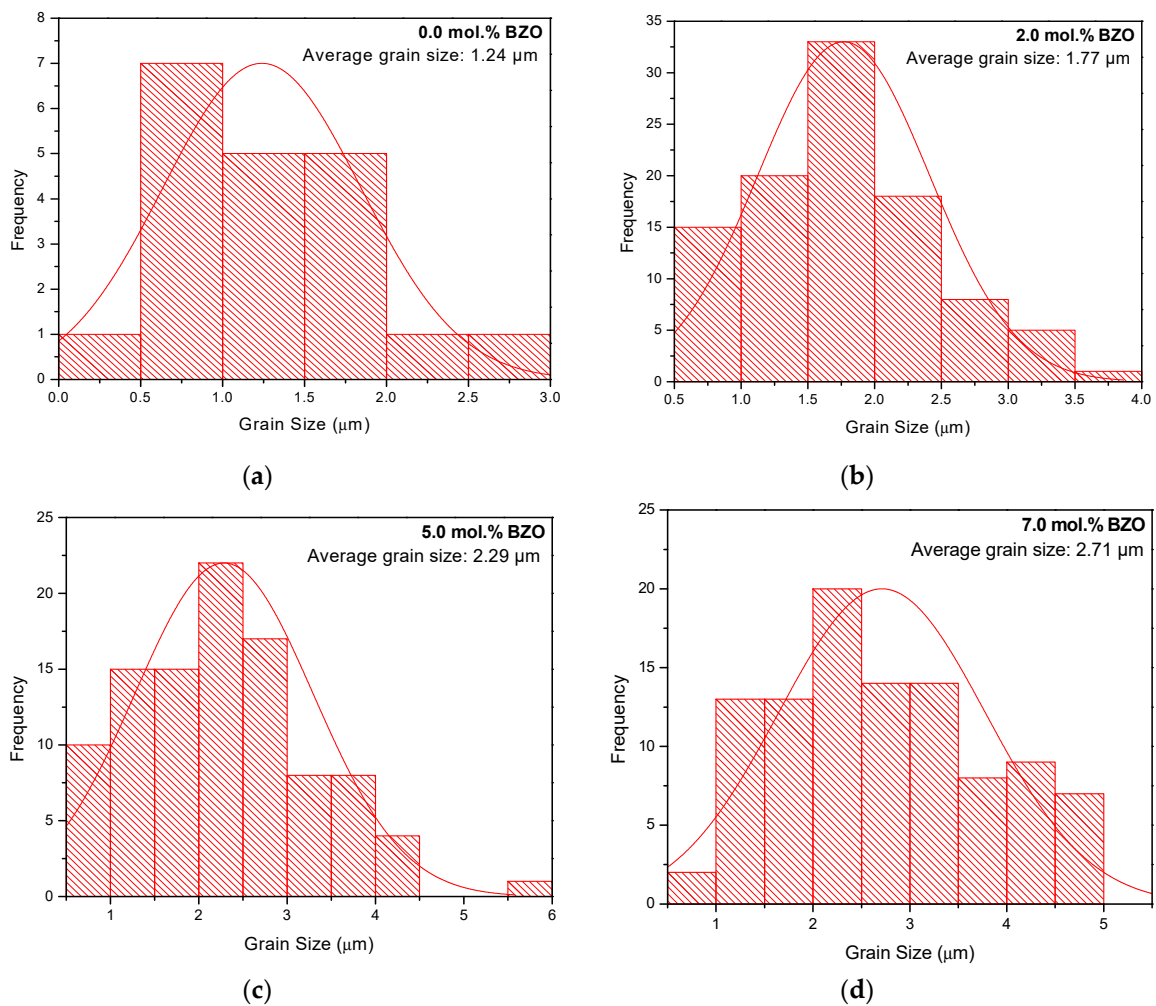

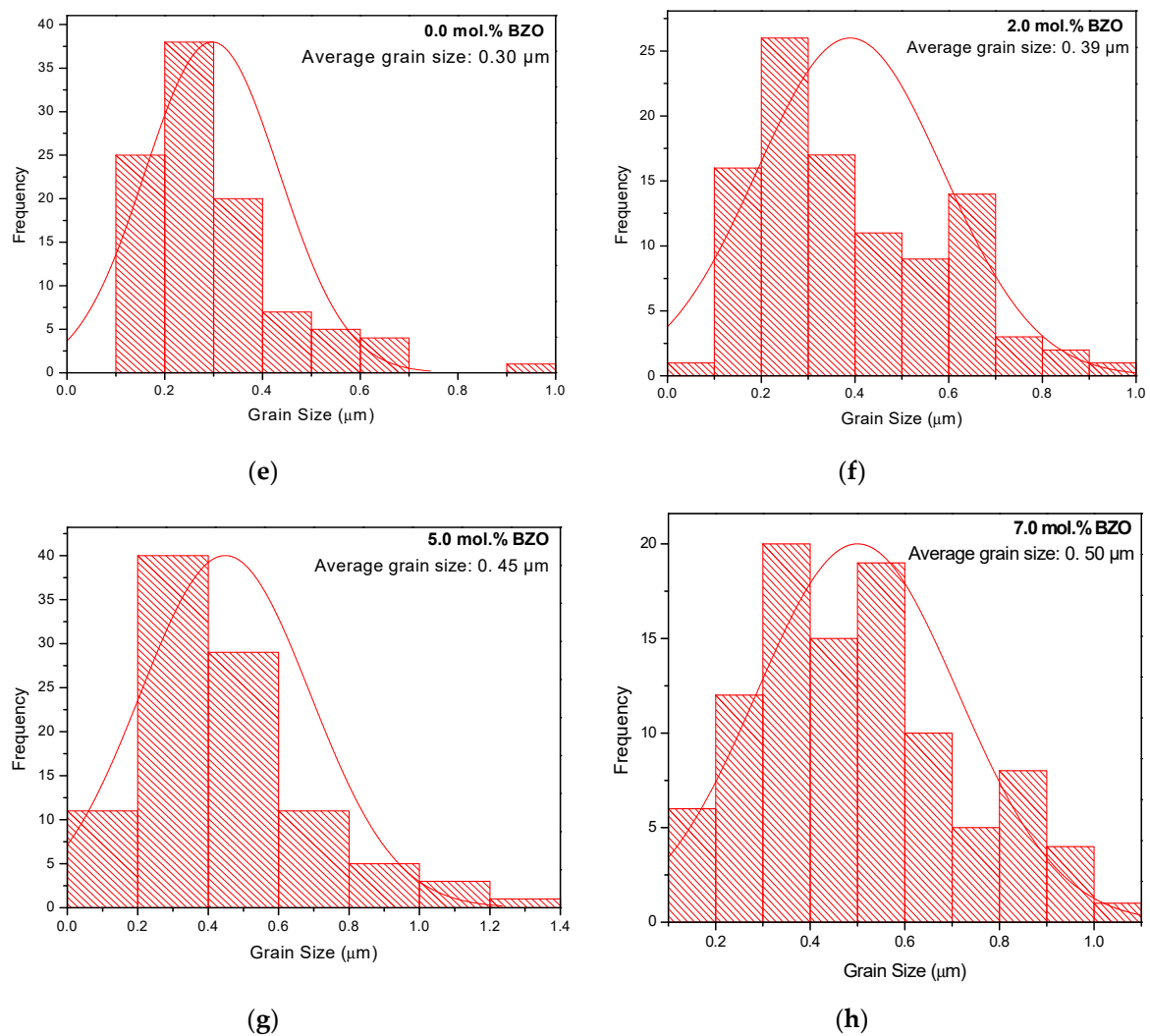**Figure 3.** *Cont.*

(e)

(f)

(g)

(h)

Figure 3. Distribution of average grain size for Y-123 added with (**a**) 0.0 mol%, (**b**) 2.0 mol%, (**c**) 5.0 mol%, and (**d**) 7.0 mol% of BZO prepared via SS method and Y-123 added with (**e**) 0.0 mol%, (**f**) 2.0 mol%, (**g**) 5.0 mol%, and (**h**) 7.0 mol% of BZO prepared via COP method.

3.3. Superconducting Properties

Figure 4 shows the temperature dependence of the real (χ') and imaginary (χ'') parts of AC susceptibility (ACS) for all the samples. The real part (χ') shows two transitions labeled as onset critical temperature, $T_{c\text{-onset}}$ and phase lock-in temperature, T_{cj}. $T_{c\text{-onset}}$ is due to transition within the grains (intra-grain) while T_{cj} is due to superconducting coupling between grains (inter-grain) [32]. In the temperature range between $T_{c\text{-onset}}$ and T_{cj}, the superconducting grains are decoupled and the sample as a whole becomes resistive even if all individual grains are still strongly superconducting. Below T_{cj}, the grains are coupled or phase-locked in which the phase difference across the intergranular junctions is zero. Consequently, the induced current from the externally applied ac magnetic field gives rise to shielding currents along the outermost surface of the sample. $T_{c\text{-onset}}$ and T_{cj} were determined from the peaks of the derivative of normalized χ', $\delta\chi'/\delta T$ against temperature, T plots (insets). It should also be noted that samples with approximately the same size (cross-section 0.3×0.5 cm) were used for measurements under the same conditions for the sake of consistency.
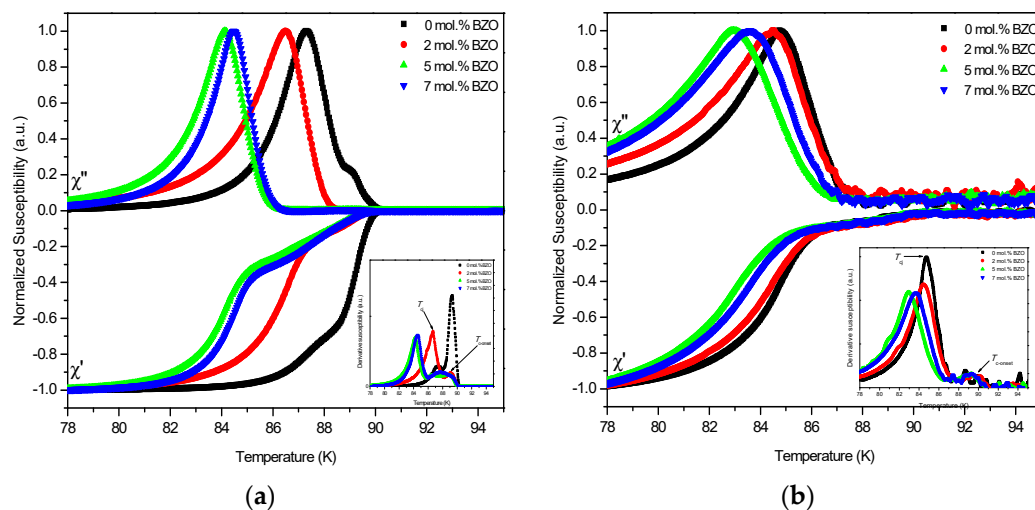
Figure 4. Temperature dependence of ACS for Y-123 + *x* mol% of BZO samples prepared via (**a**) SS method (**b**) COP method. Insets show the derivative of normalized χ', $\delta\chi'/\delta T$ against temperature, T.

Table 3 shows that the values of $T_{\text{c-onset}}$ and T_{cj} for the COP samples are close to that of the SS samples. The difference for $T_{\text{c-onset}}$ and T_{cj} is ≤1.6 K and ≤1.2 K, respectively. With increasing of BZO addition from 0.0 mol% to 7.0 mol%, $T_{\text{c-onset}}$ and T_{cj} for the COP samples decreased slightly (0.7 K and 0.8 K for $T_{\text{c-onset}}$ and T_{cj}, respectively). Nevertheless, addition of 2 mol% BZO did not change the value of T_{cj}. The marginal decrease of $T_{\text{c-onset}}$ is in good agreement with the previous finding [12,33,34] and could be associated with the reduced hole concentration [23]. However, the values of $T_{\text{c-onset}}$ and T_{cj} for the SS samples showed a larger change compared to the COP samples. For the SS samples, $T_{\text{c-onset}}$ decreased from 90.3 K for 0.0 mol% to 88.9 K for 7.0 mol% BZO addition (1.4 K). The lower $T_{\text{c-onset}}$ of the 7.0 mol% BZO added SS sample compared to that of the COP sample may be attributed to inhomogeneity of the former. Meanwhile, the value of T_{cj} decreased from 87.8 K for 0.0 mol% to 85.5 K for 7.0 mol% BZO addition (2.3 K). The decrease of T_{cj} with the increasing of BZO addition for both COP and SS samples indicates weakening of intergranular coupling perhaps due to the increasing of impurities at the grain boundaries [35,36]. However, the larger decrease of T_{cj} in the SS samples implies more severe degradation of grain coupling caused by BZO addition compared to the COP samples.

Table 3. Coupling peak temperature, T_{p}, onset critical temperature, $T_{\text{c-onset}}$, phase lock-in temperature, T_{cj}, and Josephson current, I_{o} for Y-123 + *x* mol% of BZO samples in applied AC field of 0.5 Oe.

BZO *x* (mol%)	SS Method				COP Method			
	T_{p} (K)	$T_{\text{c-onset}}$ (K)	T_{cj} (K)	I_{o} (µA)	T_{p} (K)	$T_{\text{c-onset}}$ (K)	T_{cj} (K)	I_{o} (µA)
0.0	87.3	90.3	87.8	51.21	84.8	90.6	86.6	31.69
2.0	85.8	88.9	86.6	53.95	84.5	90.5	86.5	32.08
5.0	84.1	89.9	85.4	28.20	82.9	89.8	85.6	30.56
7.0	84.5	88.9	85.5	36.49	83.6	89.9	85.8	30.54

Imaginary part (χ'') of ACS exhibits a broad peak known as coupling peak temperature, T_{p} that corresponds to the hysteretic energy dissipation as a result of AC losses at the inter-grain region [37]. The second peak near T_{c} (intra-granular peak) for all the samples is not apparent except for the pure sample prepared via the SS method. The absence of the second peak suggests that grain coupling is better for the pure sample prepared via COP method compared to the SS method [37,38]. For the COP samples, addition of 2.0 mol% of BZO did not change the T_{p} much compared to the pure sample. For the SS samples, T_{p} for the pure sample is 87.3 K compared to 85.8 K for the sample with 2.0 mol% of BZO addition. As shown in Figure 4 and Table 3, T_{p} of both the SS and COP samples shifted to lower temperature with the increasing of BZO addition due to the weakening of intergranular coupling

between the grains [39]. Other factors that affect T_p also include the changes in microstructure and the amount of impurities at the grain boundaries [40]. It is noteworthy that both T_p and T_{cj} of the 5.0 and 7.0 mol% BZO added samples are quite close to each other for the COP and SS samples. Such a small variation could be related to the saturation of solid solubility of BZO in Y-123 as mentioned in the part of XRD analysis (Section 3.1).

The value of Josephson's current, I_o was calculated according to the Ambegaokar–Baratoff theory [41] using the following equation assuming that nearest-neighbor grains are coupled by identical Josephson junctions of maximum I_o:

$$I_o = 1.57 \times 10^{-8} \left(\frac{T_{c\text{-onset}}^2}{T_{c\text{-onset}} - T_{cj}} \right) \tag{2}$$

It should be noted that Equation (2) is only valid for s-wave superconductors at temperature near to the superconducting transition temperature, T_c. Nonetheless, the equation has been adapted for the estimation of maximum Josephson current in d-wave cuprate superconductor [42]. The values of $T_{c\text{-onset}}$ and T_{cj} were estimated from Figure 4 as mentioned before. Due to the granular nature of HTS, grain boundaries of Y-123 act as Josephson junctions. In equation (2), T_{cj} represents the Josephson phase-locking temperature which is the crossover temperature between phase-locked and phase fluctuation dominated behavior, corresponding to coupling and decoupling of grains, respectively [41].

Table 3 shows that the I_o increased for 2.0 mol% samples but decreased for 5.0 mol% and 7.0 mol% BZO addition for both methods. The Josephson current, $I_o = 53.95$ µA for 2 mol% BZO added SS sample is the highest. Meanwhile, I_o for 2.0 mol% BZO added COP sample is 32.08 µA. These values are higher than that $I_o \approx 5$ µA in Bi-Ca-Sr-Cu-O bulk prepared using solid state reaction method [42]. The increasing of Josephson's current, I_o up to 2.0 mol% indicated better coupling between the grains and thus, stronger Josephson junction. Consequently, the screening current circulated even at higher field causing the increasing tunneling of Josephson current across the grain boundaries [43]. However, further addition of 5.0 mol% and 7.0 mol% BZO in the SS samples, abruptly decreased the I_o to 28.20 µA and 36.49 µA, respectively. For the COP samples, I_o decreased to 30.56 µA and 30.54 µA with addition of 5.0 and 7.0 mol% BZO, respectively. Nevertheless, the variation in I_o with increased BZO addition in the COP samples is smaller probably because of higher homogeneity over the SS samples. Such decrease in I_o is reflected in the more drastic decrease of T_{cj} of the 5.0 and 7.0 mol% BZO added samples (Table 3). This is most probably related to the distribution of BZO particles which are insulating at the grain boundaries. The same reason is believed to be accounted for the lower I_o of the COP samples compared to that of the SS samples. This can be understood by the presence of more grain boundaries in the COP samples due to smaller grain size (Table 2). Hence, tunneling of Josephine current is hindered due to the distribution of the insulating BZO particles at the grain boundaries.

4. Conclusions

In this work, structural properties of BZO doped Y-123 bulks prepared using COP and SS method, respectively, were studied and their AC susceptibility was compared. The polycrystalline samples with nominal composition of Y-123 added with x mol% of BZO nanoparticles ($x = 0.0, 2.0, 5.0$, and 7.0) were synthesized. The XRD patterns showed the formation of Y-123 as the major phase and Y-211 as the secondary phase. The COP samples showed higher weight percentage of Y-123 phase. Refinement of unit cell lattice parameters indicated that all the samples have an orthorhombic crystal structure. Estimation based on the SEM images showed that the COP samples have smaller average grain size than that of the SS samples probably because of lower sintering temperature used for the former. $T_{c\text{-onset}}$ was found to decrease with addition of BZO as shown by the ACS measurement. The value of Josephson's current, I_o increased up 53.95 µA and 32.80 µA for 2.0 mol% BZO added SS and COP samples, respectively. The lower I_o value of the COP samples compared with the SS samples is attributed to the presence of more grain boundaries. Hence, tunneling of I_o is hindered due to the distribution of insulating BZO particles at the grain boundaries.

References

1. Barnes, P.N.; Haugan, T.J.; Baca, F.J.; Varanasi, C.V.; Wheeler, R.; Meisenkothen, F.; Sathiraju, S. Inducing self-assembly of Y_2BaCuO_5 nanoparticles via Ca-doping for improved pinning in $YBa_2Cu_3O_{7-x}$. *Physica C* **2009**, *469*, 2029–2032. [CrossRef]

2. Horvath, D.; Harnois, C.; Noudem, J.G. Li and Ce doping of melt-textured YBCO: Improved J_c at medium fields. *Mater. Sci. Eng. B* **2008**, *151*, 36–39. [CrossRef]

3. Klie, R.F.; Buban, J.P.; Varela, M.; Franceschetti, A.; Jooss, C.; Zhu, Y.; Browning, N.D.; Pantelides, S.T.; Pennycook, S.J. Enhanced current transport at grain boundaries in high-T_c superconductors. *Nature* **2005**, *435*, 475–478. [CrossRef]

4. Jin, L.H.; Zhang, S.N.; Yu, Z.M.; Li, C.S.; Feng, J.Q.; Sulpice, A.; Wang, Y.; Zhang, P.X. Influences of $BaZrO_3$ particles on the microstructure and flux pinning of YBCO film prepared by using modified TFA-MOD approach. *Mater. Chem. Phys.* **2015**, *149–150*, 188–192. [CrossRef]

5. Awano, M.; Fujishiro, Y.; Moon, J.; Takagi, H.; Rybchenko, S.; Bredikhin, S. Microstructure control of an oxide superconductor on interaction of pinning centers and growing crystal surface. *Physica C* **2000**, *341–348*, 2017–2018. [CrossRef]

6. Paulose, K.V.; Koshy, J.; Damodaran, A.D. Superconductivity in $YBa_2Cu_3O_{7-\delta}$-ZrO_2 systems. *Supercond. Sci. Technol.* **1991**, *4*, 96–101. [CrossRef]

7. Palonen, H.; Huhtinen, H.; Shakhov, M.A.; Paturi, P. Electron mass anisotropy of $BaZrO_3$ doped YBCO thin films in pulsed magnetic fields up to 30 T. *Supercond. Sci. Technol.* **2013**, *26*, 045003. [CrossRef]

8. Bretos, I.; Schneller, T.; Falter, M.; Backer, M.; Hollmann, E.; Wordenweber, R.; Molina-Luna, L.; Tendeloo, G.V.; Eibl, O. Solution-derived $YBa_2Cu_3O_{7-\delta}$ (YBCO) superconducting films with $BaZrO_3$ (BZO) nanodots based on reverse micelle stabilized nanoparticles. *J. Mater. Chem. C* **2015**, *3*, 3971–3979. [CrossRef]

9. Peurla, M.; Paturi, P.; Stepanov, Y.P.; Huhtinen, H.; Tse, Y.Y.; Bodi, A.C.; Raittila, J.; Laiho, R. Optimization of the $BaZrO_3$ concentration in YBCO films prepared by pulsed laser deposition. *Supercond. Sci. Technol.* **2006**, *19*, 767–771. [CrossRef]

10. Malmivirta, M.; Rijckaert, H.; Paasonen, V.; Huhtinen, H.; Hynninen, T.; Jha, R.; Awana, V.S.; Driessche, I.V.; Paturi, P. Enhanced flux pinning in YBCO multilayer films with BCO nanodots and segmented BZO nanorods. *Sci. Rep.* **2017**, *7*, 14682. [CrossRef]

11. Wang, F.; Tian, H. $BaZrO_3$ (BZO) nanoparticles as effective pinning centers for -$YBa_2Cu_3O_{7-\delta}$ (YBCO) superconducting thin films. *J. Mater. Sci. Mater. Electron.* **2019**, *30*, 4137–4143. [CrossRef]

12. Jha, A.K.; Khare, N. Investigation of flux pinning properties of YBCO: $BaZrO_3$ composite superconductor from temperature dependent magnetization studies. *J. Magn. Magn. Mater.* **2010**, *322*, 2653–2657. [CrossRef]

13. Arlina, A.; Halim, S.A.; Awang Kechik, M.M.; Chen, S.K. Superconductivity in Bi-Pb-Sr-Ca-Cu-O ceramics with YBCO as additive. *J. Alloys Compd.* **2015**, *645*, 269–273. [CrossRef]

14. Paz-Pujalt, G.R.; Mehrotra, A.K.; Ferranti, S.A.; Agostinelli, J.A. Solid state reactions in the formation of $YBa_2Cu_3O_{7-\delta}$ high T_c superconductor powders. *Solid State Ionics* **1989**, *32–33*, 1179–1182. [CrossRef]

15. Fujihara, S.; Kozuka, H.; Yoko, T.; Sakka, S. Mechanism of formation of $YBa_2Cu_4O_8$ superconductor in the sol-gel synthesis. *J. Sol-Gel Sci. Technol.* **1994**, *1*, 133–140. [CrossRef]

16. Ramli, A.; Halim, S.A.; Chen, S.K.; Awang Kechik, M.M. The effect of Gd_2O_3 nanoparticles addition on microstructural and electrical properties of YBCO superconductor. *ARPN J. Eng. Appl. Sci.* **2016**, *11*, 13708–13715.

17. Hamadneh, I.; Rosli, A.M.; Abd-Shukor, R.; Suib, N.R.M.; Yahya, S.Y. Superconductivity of $REBa_2Cu_3O_{7-\delta}$ (RE = Y, Dy, Er) ceramic synthesized via coprecipitation method. *J. Phys. Conf. Ser.* **2008**, *97*, 012063. [CrossRef]

18. Bhargava, A.; Mackinnon, I.D.R.; Yamashita, T.; Page, D. Bulk manufacture of YBCO powders by coprecipitation. *Physica C* **1995**, *241*, 53–62. [CrossRef]

19. Mousa Dihom, M.; Shaari, A.H.; Baqiah, H.; Al-Hada, N.M.; Talib, Z.A.; Chen, S.K.; Aziz, R.S.; Awang Kechik, M.M.; Lim, K.P.; Shukor, R.A. Structural and superconducting properties of $Y(Ba_{1-x}K_x)_2Cu_3O_{7-\delta}$ ceramics. *Ceram. Int.* **2017**, *43*, 11339–11344. [CrossRef]

20. Wahid, M.H.; Zainal, Z.; Hamadneh, I.; Tan, K.B.; Halim, S.A.; Rosli, A.M.; Alaghbari, E.S.; Nazarudin, M.F.; Kadri, E.F. Phase formation of $REBa_2Cu_3O_{7-\delta}$ (RE: $Y_{0.5}Gd_{0.5}$, $Y_{0.5}Nd_{0.5}$, $Nd_{0.5}Gd_{0.5}$) superconductors from nanopowders synthesised via co-precipitation. *Ceram. Int.* **2012**, *38*, 1187–1193. [CrossRef]

21. Ochsenkuhn-Petropoulou, M.; Argyropoulou, R.; Tarantilis, P.; Kokkinos, E.; Ochsenkuhn, K.M.; Parissakis, G. Comparison of the oxalate co-precipitation and the solid state reaction methods for the production of high temperature superconducting powders and coating. *J. Mater. Process. Technol.* **2002**, *127*, 122–128. [CrossRef]

22. Mohd Hapipi, N.; Chen, S.K.; Shaari, A.H.; Awang Kechik, M.M.; Tan, K.B.; Lim, K.P. Superconductivity of Y_2O_3 and $BaZrO_3$ nanoparticles co-added $YBa_2Cu_3O_{7-\delta}$ bulks prepared using co-precipitation method. *J. Mater. Sci. Mater. Electron.* **2018**, *29*, 18684–18692. [CrossRef]

23. Mohd Hapipi, N.; Chen, S.K.; Shaari, A.H.; Awang Kechik, M.M.; Tan, K.B.; Lim, K.P.; Lee, O.J. AC susceptibility of $BaZrO_3$ nanoparticles added $YBa_2Cu_3O_{7-\delta}$ superconductor prepared via coprecipitation method. *J. Supercond. Novel Magn.* **2018**, *32*, 1191–1198. [CrossRef]

24. Patnaik, P. *Dean's Analytical Chemistry Handbook*, 2nd ed.; McGraw Hill Professional: New York, NY, USA, 2004.

25. Zhang, C.J.; Oyanagi, H. The synthesis condition and its influence on T_c in Mn doped $La_{1.85}Sr_{0.15}CuO_4$. *Physica C* **2008**, *468*, 1155–1158. [CrossRef]

26. Pomar, A.; Vlad, V.R.; Llordes, A.; Palau, A.; Gutiérrez, J.; Ricart, S.; Puig, T.; Obradors, X.; Usoskin, A. Enhanced vortex pinning in YBCO coated conductors with BZO nanoparticles from chemical solution deposition. *IEEE Trans. Appl. Supercond.* **2009**, *19*, 3258–3261. [CrossRef]

27. Cracolice, M.S.; Peters, E.I. *Introductory Chemistry: An Active Learning Approach*; Brooks Cole: Belmont, CA, USA, 2012.

28. Langford, J.I.; Wilson, A.J.C. Scherrer after sixty years: A survey and some new results in the determination of crystallite size. *J. Appl. Crystallogr.* **1978**, *11*, 102–113. [CrossRef]

29. Hassanzadeh-Tabrizi, S.A.; Mazaheri, M.; Aminzare, M.; Sadrnezhaad, S.K. Reverse precipitation synthesis and characterization of CeO_2 nanopowder. *J. Alloys Compd.* **2010**, *491*, 499–502. [CrossRef]

30. Mondal, O.; Pal, M.; Singh, R.; Sen, D.; Mazumder, S.; Pal, M. Influence of doping on crystal growth, structure and optical properties of nanocrystalline $CaTiO_3$: A case study using small-angle neutron scattering. *J. Appl. Crystallogr.* **2015**, *48*, 836–843. [CrossRef]

31. Luo, Y.Y.; Wu, Y.C.; Xiong, X.M.; Li, Q.Y.; Gawalek, W.; He, Z.H. Effects of precursors with fine $BaZrO_3$ inclusions on the growth and microstructure of textured YBCO. *J. Supercond.* **2000**, *13*, 575–581. [CrossRef]

32. Nikolo, M. Superconductivity: A guide to alternating current susceptibility measurements and alternating current susceptometer design. *Am. J. Phys.* **1995**, *63*, 57–65. [CrossRef]

33. Ciontea, L.; Celentano, G.; Augieri, A.; Ristoiu, T.; Suciu, R.; Gabor, M.S.; Rufoloni, A.; Vannozzi, A.; Galluzi, V.; Petrisor, T. Chemically processed $BaZrO_3$ nanopowders as artificial pinning centres. *J. Phys. Conf. Ser.* **2008**, *97*, 012289. [CrossRef]

34. MacManus-Driscoll, J.L.; Foltyn, S.R.; Jia, Q.X.; Wang, H.; Serquis, A.; Civale, L.; Maiorov, B.; Hawley, M.E.; Maley, M.P.; Peterson, D.E. Strongly enhanced current densities in superconducting coated conductors of $YBa_2Cu_3O_{7-x}$ + $BaZrO_3$. *Nat. Mater.* **2004**, *3*, 439–443. [CrossRef] [PubMed]

35. Kameli, P.; Salamati, H.; Eslami, M. The effect of sintering temperature on the intergranular properties of Bi2223 superconductors. *Solid State Commun.* **2006**, *137*, 30–35. [CrossRef]

36. Nedkov, I.; Veneva, A. Grain boundaries contribution to the complex susceptibility of KCu-doped YBCO high-temperature superconductors. *J. Low Temp. Phys.* **1997**, *107*, 497–502. [CrossRef]

37.	Deac, I.G.; Burzo, E.; Pop, A.V.; Pop, V.; Tetean, R.; Kovacs, D.; Borodi, G. Intergranular properties of $(Y_{1-x-y}Zr_xCa_y)Ba_2Cu_3O_{7-\delta}$ compounds. *Int. J. Mod. Phys. B* **1999**, *13*, 1645–1654. [CrossRef]

38.	Sbarciog, C.; Redac, R.T.; Deac, I.G.; Pop, I. Intergranular properties of Zr-substituted Y123 compounds. *Mod. Phys. Lett. B* **2006**, *20*, 1191–1198. [CrossRef]

39.	Rani, P.; Jha, R.; Awana, V.P.S. AC susceptibility study of superconducting $YBa_2Cu_3O_7$: Ag_x bulk composites (x = 0.0–0.20): The role of intra and intergranular coupling. *J. Supercond. Novel Magn.* **2013**, *26*, 2347–2352. [CrossRef]

40.	Nur-Akasyah, J.; Nur-Shamimie, N.H.; Abd-Shukor, R. Effect of CdTe addition on the electrical properties and AC susceptibility of $YBa_2Cu_3O_{7-\delta}$ superconductor. *J. Supercond. Novel Magn.* **2017**, *30*, 3361–3365. [CrossRef]

41.	Clem, J.R. Granular and superconducting-glass properties of the high-temperature superconductors. *Physica C* **1988**, *153–155*, 50–55. [CrossRef]

42.	Emmen, J.H.P.M.; Brabers, V.A.M.; De Jonge, W.J.M.; Steen, C.V.D.; Dalderop, J.H.J.; Geppaart, P.M.A.; Kopinga, K. Microstructure and properties of Bi-Ca-Sr-Cu-O superconductors. *J. Less-Common Met.* **1989**, *151*, 63–69. [CrossRef]

43.	Narlikar, A.V. *Field Penetration and Magnetization of High Temperature Superconductors*; Nova Science Publisher, Inc.: New York, NY, USA, 1995.